Heliyon 10 (2024) e27639

Contents lists available at ScienceDirect

Heliyon

journal homepage: www.cell.com/heliyon

Research article

Effect of successive recycling and reuse of acid liquor for the synthesis of graphene oxides with higher oxygen-to-carbon ratios

Mohammad Amirul Hoque [a,*], A.F.M. Mustafizur Rahman [b], Mohammad Mahbubur Rahman [a], Mohammad Nazrul Islam Bhuiyan [c], Shirin Akter Jahan [d], Md Aftab Ali Shaikh [a,e], Mohammad Nurnabi [b,**]

[a] BCSIR Dhaka Laboratories, Bangladesh Council of Scientific and Industrial Research (BCSIR), Dhanmondi, Dhaka, 1205, Bangladesh
[b] Department of Applied Chemistry and Chemical Engineering, University of Dhaka (DU), Dhaka, 1000, Bangladesh
[c] Institute of Food Science and Technology, Bangladesh Council of Scientific and Industrial Research (BCSIR), Dhanmondi, Dhaka, 1205, Bangladesh
[d] Institute of Glass and Ceramic Research and Testing, Bangladesh Council of Scientific and Industrial Research (BCSIR), Dhanmondi, Dhaka, 1205, Bangladesh
[e] Department of Chemistry, University of Dhaka (DU), Dhaka, 1000, Bangladesh

ARTICLE INFO

Keywords:
Graphene oxides
Reduced graphene oxides
Acid recovery
Acid reuse
Chemical oxidation
Graphene

ABSTRACT

Graphene has recently drawn exponential attention due to its surprising physicochemical properties and diversified field of applications. Although graphene oxides (GOs), itself is an exclusive material, it is also an intermediate product for the production of reduced graphene oxides (rGOs), graphene and their derivatives, which are other more superficial materials. In this study, GOs with higher oxygen to carbon ratios were synthesized following the Tour method, where the excess feed acid liquor (FAL) of mixed concentrated sulfuric and orthophosphoric acids at a ratio of 90:10 was recovered from the reaction slurries by applying the centrifugation technique. About 80–90 % of the FAL was recycled and reused as feed for the subsequent batches. The changes in the properties of FAL for the five consecutive recycling and reuse were studied. The properties of recycled FALs were investigated by measuring density, moisture content, pH, and ion concentration. The consecutive recycling of FALs tends to increase the moisture content about 0.5% in each recycles. Ion-chromatography (IC) was used to measure the variation in SO_4^{2-} and PO_4^{3-} ions in the FALs. The H_2SO_4 reacts with $KMnO_4$ and crystalized out from the recovered FAL faster than the phosphoric acid. So, sulfuric acid content in the makeover FALs must be greater than primary FAL. The product GOs were characterized using FT-IR, FT-Raman, UVVis, STA, SEM, XPS, Zeta-potential, and particle size analyzers. The variation of the properties of GOs with the changes in the reaction parameters such as temperature and time were investigated and correlated with the product yield. It was observed that the effect of temperature on the reaction rate was found to be negatively and positive with the reaction time. The oxygen-to-carbon atomic ratio from XPS analysis was found 66.7%, which supported the increase in product yields 66.9% in the experimental results. The effect of acid concentration, reaction temperature, and time on the GOs properties were satisfactory, correlated, and easily controllable with the reaction conditions. A

* Corresponding author. Fibre & Polymer Research Division, BCSIR Dhaka Laboratories, Dhanmondi, Dhaka, 1205, Bangladesh.
** Corresponding author. Department of Applied Chemistry and Chemical Engineering, University of Dhaka (DU), Shahbag, Dhaka, 1000, Bangladesh.
E-mail addresses: amirul.bcsir@yahoo.com (M.A. Hoque), mustafizacce@du.ac.bd (A.F.M.M. Rahman), mahbub.bcsir@yahoo.com (M.M. Rahman), nazrulbcsir@gmail.com (M.N.I. Bhuiyan), shirin_akterbcsir@yahoo.com (S.A. Jahan), aftabshaikh@du.ac.bd (M.A. Ali Shaikh), nnabi@du.ac.bd (M. Nurnabi).

https://doi.org/10.1016/j.heliyon.2024.e27639
Received 16 January 2024; Received in revised form 19 February 2024; Accepted 4 March 2024
Available online 9 March 2024

higher extent of oxidation and enhanced product yields 65–70% were observed at 60–70 °C and 14–18 h. A mixture of nano- and macro-molecular GOs was obtained, and their compositions were easily controllable and separable by controlling the reaction conditions. A correlation was made among the properties of synthesized GOs, FAL, and recycled FAL and reaction conditions.

1. Introduction

The term "graphene" was first introduced by A. Geim and K. Novoselov, and they were awarded the Nobel Prize in 2010 for their revolutionary contribution to discovering one carbon atom-thick two-dimensional materials that exhibit high crystal quality. They first obtained single-layer and few-layer transferable graphene nanosheets by mechanical exfoliation from graphite samples [1,2]. Chemically, graphene was observed as a two-dimensional nanomaterial, and it contains single and multi-layers of carbon atoms arranged as a honeycomb lattice that is held together by σ bonds, where most of the carbon atoms preserve sp^2 hybridization [3,4]. Generally, 2D graphene sheets are rolled into 3D graphite structure. Thus, graphene sheets need to be separated from the graphite structure. Synthesizing graphene oxides (GOs) are one of the effective ways to separate graphene from graphite lattices. Typical process of graphene separation is done by oxidizing the graphene sheets to introduce oxygen into its lattice structure followed by reduction of the GO either thermally or chemically. Moreover, GOs are an excellent starting material for the synthesis of various derivatives of graphene such as Fluorographene, graphol, graphene acid, etc. [5–7].

GOs have wide variety of applications owing to its tunable properties and relatively easy modification techniques than other conventional materials. Generally, graphite has been used as a very efficient material for energy storage devices such as batteries, capacitors, etc. [8]. Recently, reduced GOs (rGOs) are extensively used as replacement of graphite owing to their enhanced charge storage properties and large surface area compared to graphite [9,10]. GOs are also suitable for making transparent conductive films [11], strong conducting papers [12], and ultra-light elastic aerogels [13,14]. Numerous fascinating applications based on the electronic, optical, thermal, mechanical, and chemical nature of graphene and GOs have been adopted as solid electrolyte or proton conductors, electronics devices ferromagnetism, electrodes or electron mediators for enzyme biosensors, biomedical applications, surface coating technology, composites, dye-sensitized solar cells [15], paper-like materials, filters for water and purification [16], and as an ingredient of hybrid photo-catalysts in water splitting, nano-filtration membrane [17–20]. Recently, GOs have been used to avoid friction in mechanical devices due to its self-lubricating properties [21].

To eliminate difficulties in the synthesis of graphene in bulk, various chemical methods were introduced. The procedure involves the chemical oxidation of graphite to form graphene oxides (GOs) and is followed by a reduction process [22]. The Hummers' method, which is extensively employed for the chemical conversion of graphite to graphene oxide (GOs), entails an initial oxidation step utilizing $KMnO_4$, $NaNO_3$, and H_2SO_4 at a significantly reduced temperature to mitigate the risk of explosion. Subsequently, over a period of several hours, the resulting mixture is subjected to high temperatures. The Hummer's method was modified further to improve the synthesis of GOs by replacing $NaNO_3$ with K_2FeO_4. The modified Hummer's method provides comparatively better-desired properties in GOs than the Hummer's methods [23,24]. The properties of the synthesized GOs were found to be the same as those of the preferred method. In addition, the evolution of toxic gases is minimized in this process hence, it is termed as a facile synthesis approach [25,26]. Notable progress has been made in enhancing Hummer's technique for synthesizing GOs, with a focus on cost-effectiveness and efficiency. The improvement of the method is to eliminate $NaNO_3$ and replace $KMnO_4$ with K_2FeO_4. The method also reduced the use of concentrated sulfuric acid without affecting the yields, properties, or applications of GOs [27]. Synthesizing GOs in polar solvent enhances the conductivity of the GO sheets [28].

This method was further improved by James M. Tour, and is termed the Tour's method. This process excludes the use of $NaNO_3$ with the increase in the amount of $KMnO_4$ in the presence of mixed acid (MA), H_2SO_4/H_3PO_4 with a ratio of 9:1. The presence of orthophosphoric acid improves the efficiency of the oxidation process. This method yields more hydrophilic GOs compared to other methods. Moreover, this method does not generate toxic gas, and the temperature is moderately higher than room temperature, making it easy to control [29]. A higher amount of oxygen-containing GOs can be obtained by this method than by other chemical methods [30]. The roles of SO_4^{2-} ions in GO synthesis were investigated, and it was found that the formation of the epoxy bridge between the nearby carbon atoms increases with ion concentration [31]. The Tour method underwent further enhancements with the incorporation of a pre-treatment procedure applied to the graphite raw materials prior to the oxidation stage. This modification led to notable enhancements in the properties of the synthesized GOs [32]. An effective condition for the preparation of few-layered GOs and rGOs was thoroughly investigated, and the properties of the prepared products were evaluated. The degree of oxidation was controlled by varying reaction times and temperatures, and the interlayer distances of few-layer graphene were found to increase with increasing time and temperature [33]. In another study, GOs were alternatively synthesized from graphite using low concentration of ozone at high temperature which produced GOs with enhanced properties [34]. Moreover, the material is highly stable at slightly elevated temperatures. The exposure of GO materials and composites to very high temperatures initiate a degradation process that results in a change in color shade [35,36].

However, notable limitations are associated with the various chemical techniques employed in the synthesis of GOs. These include high costs, time-consuming reactions, difficulties in controlling process parameters, the risk of explosions, environmental pollution, the generation of numerous byproducts, the inclusion of contaminants requiring further purification, and imprecise control of the degree of oxidation and particle size [37,38]. To reduce these difficulties, an effective method of electrochemical exfoliation of graphite was established [39]. This method reports a scalable, safe, and environmentally friendly approach with a high yield [39,40].

The reactions of graphite to GOs are based on electrolytic oxidation conditions in water. In the electrochemical oxidation method, the graphite lattice is fully oxidized within a few seconds making it a very fast process [40]. The GOs obtained by this method have similar properties as those of the other methods. The synthesis method is continuous and easily controllable. Another approach to reduce the difficulties of the production of GOs from graphite was using $KFeO_4$ instead of $KMnO_4$ with concentrated H_2SO_4. This method not only minimizes environmental pollution but also reduces reaction times from several hours/days to only 1 h. The produced GOs powders are highly water-soluble, from which GOs liquid crystals can be formed, and thus macroscopic graphene fibers, films, and aerogels can be produced. This method produces 100% of single-layered GOs and their macroscopic materials without applying any ultrasonic treatment. Thus, the large-scale commercial production of graphene becomes ultra-low-cost [41,42]. GOs are also synthesized by applying ultrasonication to reduce cost and impurities [43,44]. GOs can be reduced using a number of reducing chemicals, such as ascorbic acid and hydrazine [45].

Economical and environmentally friendly synthesis methods of GOs are essential for industrial applications. Several studies have focused on developing economical and green synthesis techniques for GOs and rGOs. Green synthesis involves the use of natural and biochemicals such as plant extracts and biomass for the reduction and stabilization of rGOs [46,47]. Although these methods are environmentally friendly, they are impractical in industrial setting. Synthesis of GOs in the Hummer's, modified Hummer's, and Tour method is highly effective and applicable in industrial environment. Among these methods, Tour method of synthesizing GOs is industrially favorable, energy efficient, and ecofriendly [48,49]. Moreover, oxygen to carbon ratio of GOs are much higher in Tour's method than any other synthesis techniques. However, recycling and reusing the reagents for successive synthesis of GOs can increase its sustainability and add more value as an ecofriendly technique. To this date, very few studies have been reported on the successive use of chemical reagents for producing GOs with high oxygen to carbon ratio.

In this research, GOs have been synthesized by the oxidation of graphite using the Tour's method. The unreacted feed acid liquors (FAL) have been recycled and reused for five consecutive cycles. The recycled FAL and synthesized GOs have been characterized using state-of-the-art instruments. A correlation has been established between the properties of recycled FAL and synthesized GOs.

2. Methods

2.1. Materials

The chemicals used for the experiment were collected from the following sources: Extra pure graphite fine powder of purity 98% with particle size 60 mesh was collected from Loba Chemie Pvt. Ltd., Mumbai, India; reagent grade potassium permanganate with purity 99.8%; AR grade sulfuric acid with purity 97%; reagent grade hydrochloric acid with purity −37%; and AR grade hydrogen peroxide with purity 35% were from Merck KGaA, Darmstadt, Germany; and AR grade orthophosphoric acid with purity 85% from Active Fine Chemicals Ltd., Dhaka, Bangladesh.

2.2. Karl-Fischer moisture analyzer

Water content in raw concentrated sulfuric acid, phosphoric acid, fresh MA, and recovered acid liquors after every reaction was measured by using a Karl-Fischer moisture analyzer (Metrohm, USA). For each measurement, 0.20 mL of sample was put to a moisture-free Karl-Fischer reagent. The acquired data were expressed as percentages [50].

2.3. Measurement of anions content

Ion chromatography (Thermo Scientific, Germany) was utilized for the measurement of SO_4^{2-} and PO_4^{3-} ion concentrations in concentrated sulfuric acid, phosphoric acid, fresh MA, and recovered acid liquors after each reaction. After adjusting the concentration to the calibration range, 0.10 mL of the acids were diluted to 100 mL with distilled DI water and investigated for SO_4^{2-} and PO_4^{3-} ion concentrations. The results obtained with this machine are based on ppm units [51].

2.4. Atomic absorption spectroscopy

The K^+ and Mn^{2+} ion concentrations in H_2SO_4, H_3PO_4, new MA, and recovered acid liquors were measured using atomic absorption spectroscopy (Shimadzu, Japan). After adjusting the concentration to the calibration range, 0.10 mL of the acids were diluted to 100 mL with distilled DI water and tested for K^+ and Mn^{2+} ion concentrations.

2.5. FT-IR spectroscopic analysis

The structural characterization of the G and prepared GO was carried out by attenuated total reflectance-fourier transform-infrared spectroscopy (FTIR-ATR, USA). The FT-IR spectra were captured using an ATR module with a diamond crystal. Acetone was used to polish the diamond crystal, and a background scan was taken before every measurement. The spectra were recorded in the 650–4000 cm^{-1} range at 4 cm^{-1} spectral resolution with 12 scans per spectrum.

2.6. UVvisible spectroscopic analysis

The absorbance of UVvisible light and the determination of the maximum absorbance (λ max) were carried out through the utilization of a PerkinElmer Lambda 35 instrument (USA) in the process of ultravioletvisible spectroscopy (UVVis). The powder samples were dissolved in distilled and deionized (DI) water at a concentration of approximately 1.5 mg/mL. Subsequently, the aforementioned solutions were transferred into sample cuvettes in order to conduct absorbance measurements.

2.7. DLS measurement

Particle size and zeta-potential value of the samples were measured in a particle size analyzer (Malvern, UK). Powder samples were scattered in distilled and DI water in a 0.5% ratio and placed in sample cells to measure their particle size and zeta potential.

2.8. Image analysis

Scanning Electron Microscopy-Energy Dispersive X-Ray (SEM-EDX) analyzer was used for imaging purposes (JEOL, Japan). A very small sample, about 1 mg, was placed in the sample holder and placed in the vacuum dryer at 55 °C for 12 h, and then it was placed inside the instrument for capturing the images.

2.9. XPS analysis

The X-ray photoelectron spectrum was measured using XPS spectroscopy (Bruker, USA). Powder samples were dissolved in isopropyl alcohol and derided on the copper plate to form a film. Then the sample was placed under ultrahigh vacuum in a nitrogen environment to remove atmospheric oxygen. Then the sample was analyzed to measure the binding energy of the elements.

2.10. Measurements of thermal properties

The thermal properties of graphene (G) and graphene oxides (GOs) were determined using a simultaneous thermal analyzer (Brand: Netzsch GmbH, Model: STA 449 F3 Jupiter). Approximately 3.0 mg of the samples were loaded into an alumina crucible and then positioned in the furnace. The samples were subjected to heating at a rate of 10 °C per minute, and the resulting thermogram and mass loss were recorded simultaneously.

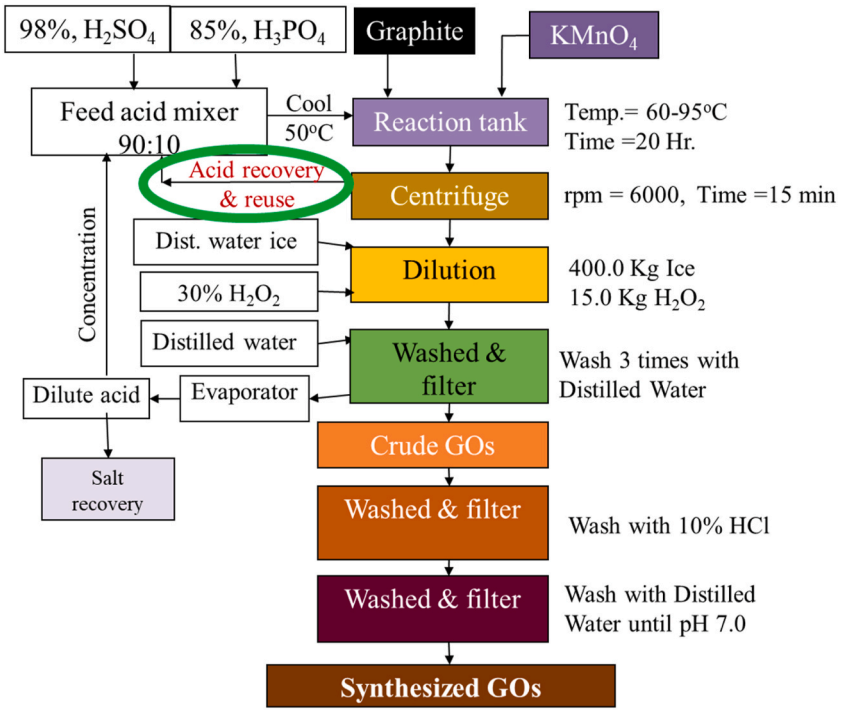

Fig. 1. Synthesis of GOs and reuse of feed acid liquor.

2.11. Synthesis of graphene oxides

Graphene oxides (GOs) were synthesized using a sequential methodology. A flat-bottom flask with a capacity of 1000 mL was initially filled with a concentrated MA solution, which was termed as feed acid liquor (FAL), approximately 1000 mL in volume. The FAL was prepared by combining concentrated H_2SO_4 and ortho H_3PO_4 in a ratio of 90:10. In order to establish a regulated environment, the flask was subjected to a cooling process, resulting in a temperature lower than 50 °C. Following that, a quantity of 10.0 g of G powder was added to the flask under constant stirring at a rate of 500 rpm. This stirring was done to prevent the formation of lumps and to ensure thorough and uniform mixing. The flask was immersed in a water bath in order to facilitate heat dissipation and control the temperature of the reaction vessel at the desired level. Following that, a total of 60.0 g of $KMnO_4$ was slowly added to the mixture with constant stirring. Subsequent to obtain the condition the temperature of the reaction media was gradually raised by 10 °C/h until 95 °C. The processes of heating and stirring were then stopped. After being cooled to room temperature, the unreacted acid solution was separated from the solid reaction mass by a centrifugation process at a speed of 6000 rpm for 20 min. The reaction mass was allowed to oxidize in air for overnight. To obtain the diluted mass a 400 g of distilled deionized water ice was added to the cake. Then a solution containing 15–30 mL of H_2O_2 with a concentration of 36% was gradually added to the mixture while maintaining a constant stirring. Under completion of oxidation process the GOs underwent a purifying step the procedure entailed filtration utilizing Whatman filter paper number-1, followed by multiple rinses with distilled deionized water and further filtration. The filtrates that were obtained were subjected to concentration in order to recover the potassium and manganese salts, which are by-products resulting from the oxidation reaction. The produced GOs filter cakes containing potassium and manganese salts also underwent a purification process. They were washed with a 10% HCl solution while being stirred and heated to a temperature below 50 °C for a duration of 2 h. Subsequently, the filter cakes were washed with distilled deionized water followed by centrifugation for 8–10 times, which resulted in a solution with a pH of approximately 7.0.

3. Results

3.1. Synthesis of GOs

The flow diagram for the synthesis of GOs has been presented in Fig. 1. A modified Hummer's method modified by Tour were followed with some modification [52]. The purpose of this modification was to mitigate the creation of lumps, prevent abrupt rise in temperature which can lead to an explosion, maximize utilization of the oxidizing agents, and to employ the FAL recycling techniques. Tour's modification technique was applied to produce GOs with higher oxygen to carbon ratios with minimum drawbacks.

The reaction continued until the color of the mixture changed from a dark violet in Fig. 2 (a) to a chocolate brown color in Fig. 2 (b). This change of the mixture color indicates the complete consumption of $KMnO_4$. The reaction temperature was gradually raised to facilitate the maximum use of the oxidizing agents. Solids and FALs were separated from the slurry using filter-press and centrifugation for further synthesis cycles. Solid reaction mass oxidized under air and moisture forming a pinkish-violet color as depicted in Fig. 2 (c). To minimize the heat generated during the dilution process with distilled deionized water ice minimized the heat of dilution. The careful incorporation of H_2O_2 was conducted in order to mitigate the occurrence of excessive foam generation resulting from the release of gases. H_2O_2 was stopped adding upon the attainment of a persistent, brilliant orange-yellow color in Fig. 2 (d). From Fig. 2, the GOs were successfully oxidized and the extent of the oxidation were indicated by the change in color intensity of the mixture.

The slurry derived from the manufacturing process of GOs contains different metal salt impurities which underwent a purifying step. The purpose of the purification is to convert the metal salts in to soluble chloride salts. These salts were easily removed by filtration. The produced GOs were freeze dried to obtain fine pure GOs powder.

During the synthesis process, particularly for Run-1, the initial temperature and the temperature primarily maintained ranged between 55 and 60 °C. Over the course of 16 h, the temperature gradually increased, reaching 95 °C within 4 h, as shown in Fig. 3. The

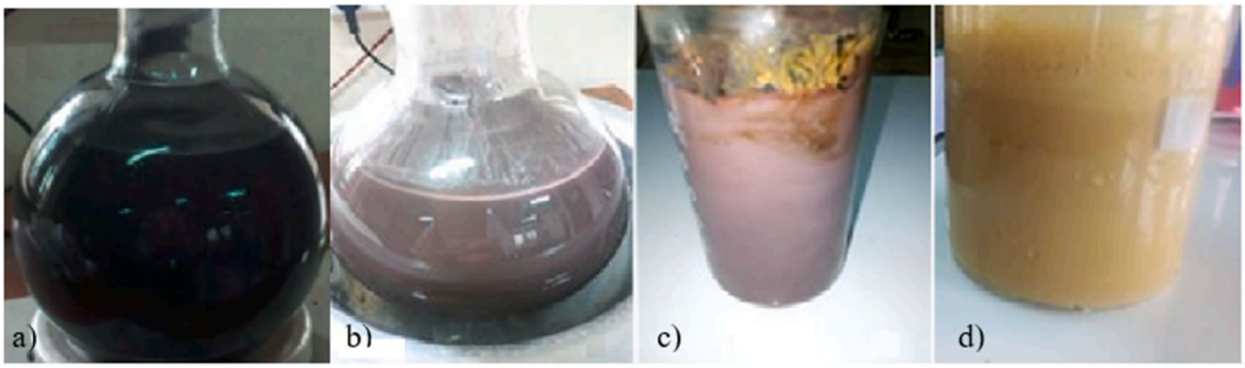

Fig. 2. Images of color changes at different stages of graphite to graphene oxide conversion. a) starting of the reaction (dark violet), b) end of the reaction (chocolate brown), c) centrifuged cake (pinkish brown), d) addition of hydrogen peroxide (golden orange). (For interpretation of the references to color in this figure legend, the reader is referred to the Web version of this article.)

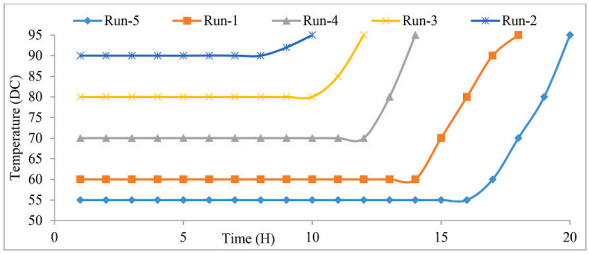

Fig. 3. Temperature profile of the experiments of Run-1, Run-2, Run-3, Run-4, and Run-5 for the synthesis of GOs with respect to time.

reaction was terminated after a total of 20 h. Similarly, for subsequent reactions, denoted as Run-2, Run-3, Run-4, and Run-5, the initial temperature and most main temperature conditions were set at 60–65, 70–75, 80–85, and 90–95 °C, respectively. The reaction durations were reduced progressively to 14, 12, 10, and 8 h for these runs, respectively.

The synthesis was carried out until the oxidizing agent was fully consumed. At 55 °C, the oxidizing agent underwent a reaction for a period of 20 h, resulting in the production of 17.05 g of GOs from an initial quantity of 10.0 g of graphite, as shown in Table 1 and Fig. 3. In a comparable manner, when subjected to 60, 70, 80, and 90 °C, the reactions exhibited reaction times of 18, 14, 12, and 10 h, respectively. Consequently, these reactions resulted in the production of 16.91 g, 16.69 g, 15.54 g, and 14.39 g of GOs, respectively.

The yield of GO production is substantially influenced by the reaction temperature and time. The oxygen content in GOs is shown to be higher when longer processes are conducted at lower temperatures, as opposed to shorter processes at higher temperatures, while maintaining the same quantity of reactants. As a consequence, there is a notable enhancement in the yields of the product inside the sediment volume, as seen from Fig. 4. As a result, decreased temperature and increased reaction time have been observed to increase the overall production yields. The most favorable reaction conditions were determined to occur within a temperature range of 65–70 °C with reaction duration of 14–15 h.

3.2. Regression analysis for GOs synthesis process

A regression study was undertaken to establish the correlation among reaction time, temperature, and the product yield of GOs in g. The analysis yielded a regression model that exhibited a high level of fit, as shown by an adjusted R^2 value of 1.00. The regression model exhibits a high level of significance ($p = 0.00$) at a significance level of 0 percent.

3.3. Regression model

Regression model obtained from the analysis is shown in equation (1)

$$\text{Product (in g)} = 37.281 - 0.204 \times \text{Temperature} + 0.450 \times \text{Time} \quad (1)$$

The regression model follows the linear straight-line equation, $Y = mX + C$. According to the model, temperature has a negative impact on product yield. With every 1 °C increase in temperature, the product yield decreases by 0.204 g. In contrast, reaction time has a positive effect on the production of GOs, contributing to a 0.45-g increase for each additional hour of reaction time, as shown in Eq 1.

The reaction involved in the oxidation process are-

3.4. Recycling of feed acid liquor

The chemical pathway involved in the synthesis of GOs increased the ratio of oxygen to carbon (Fig. 5). In the context of the oxidation reaction as a whole, it is evident that the stoichiometry indicates a 1:1 M ratio between $KMnO_4$ and H_2SO_4. Hence, a total of 60.0 g of potassium permanganate ($KMnO_4$) with a purity level of 99.8% is required to react with 39.09 g of H_2SO_4, which has a concentration of 95%. Alternatively, this can be expressed as 21.11 mL of the H_2SO_4. Nevertheless, the initial acid recovery rate remained at 86.2% during the initial run but a progressive decline in subsequent reaction cycles were observed. The observed acid consumption exceeded the anticipated theoretical value and the quantity of concentrated acids recovered exhibited a decline in successive recovery and reuse cycles. The observed phenomenon can be attributed to the absorption of acids by the solid cakes

Table 1
Properties of synthesized graphene oxides (GOs), reaction temperature, reaction time, moisture content, particle size and zeta potential value.

Experiments	Reaction temperature (°C)	Reaction time (h)	Prepared GOs (g)	Moisture content (%)	Particle Size (nm)	Zeta potential (mV)
Run-1	55	20	17.05	6.07	851	−19.7
Run-2	60	18	16.91	7.39	892	−24.1
Run-3	70	14	16.69	7.9	1013	−26.2
Run-4	80	12	15.54	8.48	1063	−29.5
Run-5	90	10	14.39	9.95	1661	−19

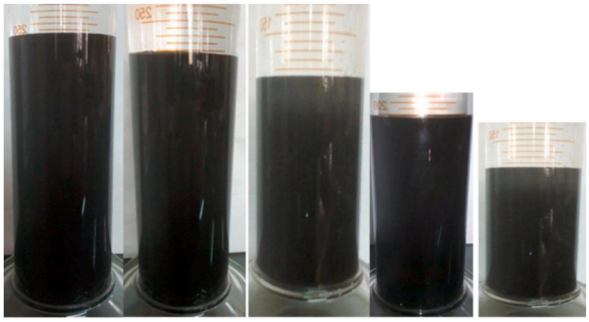

Fig. 4. Images of the sediment volume of GOs products from different reaction runs a) Run-1, volume-242 mL, b) Run-2, volume-228 mL, c) Run-3, volume- 202 mL, d) Run-4, volume-187 mL, and e) Run-5, volume-126 mL.

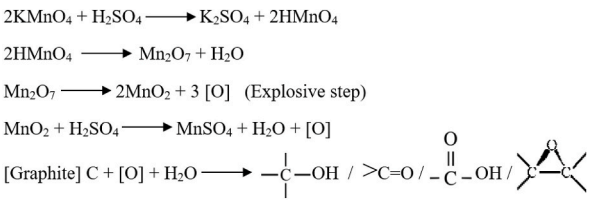

Fig. 5. Reaction mechanism for the oxidation of graphite to graphene oxide using potassium permanganate in strong acid mixture.

obtained by centrifugation of the reaction slurry. The quantity of solid cakes exhibited a gradual increase in conjunction with subsequent reactions. The cakes contained GOs as well as K, Mn, and SO_4^{2-} or PO_4^{3-} salts that precipitated from the reaction slurry as a result of saturation. As a result, there was a progressive increase in both the quantity of acid consumed and the volume of dilute acid obtained from the washing process as the number of recovery and reuse cycles increased (Fig. 6).

3.5. Moisture analysis of recycled FAL

The moisture content of the recovered MA was determined using the initial moisture content of the fresh MAs using a Karl Fischer moisture analyzer. The moisture content initially was found to be 3.77% in fresh feed acid liquor, and in recovered feed acid liquor, it gradually increased with the increasing number of recoveries and reuses. After the first recovery, it increased to 6.07% and gradually increased with the increasing number of successive recoveries and reuses, reaching 9.95% at the fifth recovery (Fig. 7). The concentration of salts in recovered FALs is also influenced by the level of moisture present in the recovered acids. The salt recovery was 58.44 g in the first recovery and gradually increased to 112.57 g in the fifth recovery. As a result, the reaction medium becomes slightly diluted but increases in density with each successive recovery and reuse (Fig. 7).

3.6. pH and density of recycled FAL

The pH of the recovered MA after dilution with water to 1:1000 also decreases, which supports the dilution of acid. However, the density of the recovered acid increases with the number of recovery cycles, as shown in Fig. 7. This is due to the increase in water

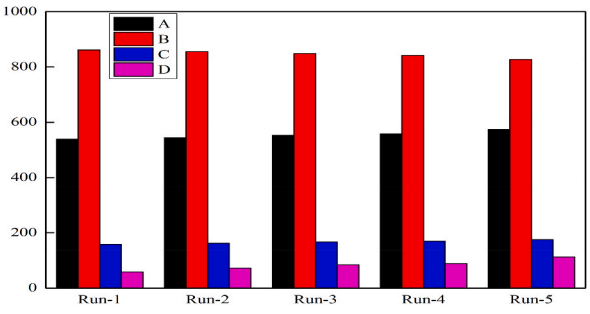

Fig. 6. Amount of consumed and recovered acid (A) MA consumed (mL), (B) recovered MA (mL), (C) recovered dilute acid (mL) and (D) recovered salt (g).

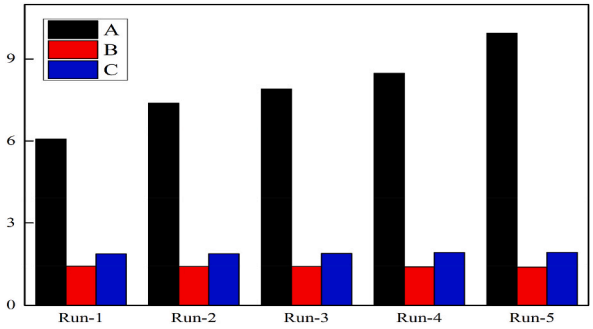

Fig. 7. Recovered acid properties (A) moisture (%), (B) pH of 0.1% water solutions, and (C) density (g/cc).

content in recovered acids, which significantly affects the solubility of salts produced in the reaction medium. Overall, the amount of recovered concentrated MA decreases with the number of runs, and the amount of recovered salts gradually increases. The absorbed acids were also collected by washing the solid cakes with a small amount of distilled water. Thus, the amount of dilute acid solutions also increased with the increasing amount of solid cakes and salts in different reaction runs (Fig. 7).

3.7. Atomic absorption spectroscopic analysis of FAL

The atomic absorption spectroscopic analysis of FAL and recycled FAL has been utilized for the measurement of K^+ and Mn^{2+} in FAL and recycled FAL [53] and is presented in Fig. 8. The amounts of K^+ and Mn^{2+} were measured with a dilution of 1:1000. Initially the K^+ ion was about 1 ppm for FAL which increased to 11.67 ppm after the first recovery, and slowly increased for successive recovery and reuse. In the case of the Mn^{2+} ion, it was 0.1 ppm for FAL and 0.53 ppm after the first recovery and increased with successive recovery and reuses [54]. After reaching around 2 ppm, it becomes saturated and does not further increase substantially.

3.8. Ion chromatographic analysis of FAL analysis of recycled FAL

The SO_4^{2-} and PO_4^{3-} ion concentrations of the FAL and recycled FAL were measured using ion chromatography after dilution to 1:1000 and are presented in Fig. 9. FAL contains 834 ppm SO_4^{2-} and is diluted after successive recovery and reuse. But in the case of phosphoric acid, the FAL contains 110 ppm, and after the first recovery, it was increased to 144 ppm and increased with recovery and reuse cycles because most of the $KMnO_4$ reacts with sulfuric acid to produce atomic oxygen and K_2SO_4 and $MnSO_4$ salts and water. Formation of PO_4^{3-} salts are prevented because of the lower affinity of K and Mn for PO_4^{3-} ions.

3.9. Synthesis of graphene oxides (GOs) with higher oxygen to carbon ratio

The synthesis of G to GOs was carried out with the varying temperature and time. At high temperatures, the reactions are completed in shorter timeframes. While at lower temperatures, reactions take more time to complete using the same amount of feed materials shown in Fig. 3. $KMnO_4$ dissociates very fast to generate atomic oxygen at high temperature so $KMnO_4$ is consumed rapidly, leading faster oxidation of the G materials. On the other hand, lower temperatures show a higher degree of oxidation of G to GOs. This process splits the G layers, which results in a reduction in particle size. The product yield is heavily dependent on the reaction temperature and time as observed from the sediment volume of the product under water presented in Fig. 4. The optimum reaction condition should be between 60 and 70 °C as seen from Fig. 10 depicting the relationship between product yield, reaction time, and temperature. The

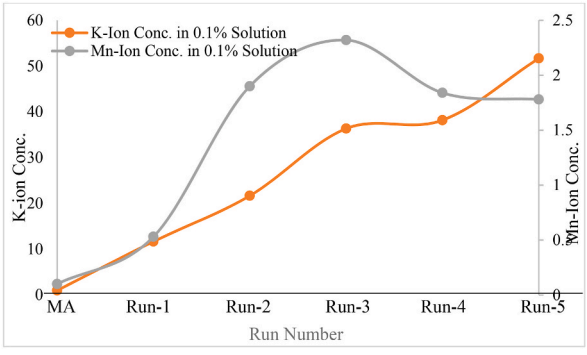

Fig. 8. K^+ and Mn^{2+} ion concentration in recovered acids after dilution to 0.1% in water.

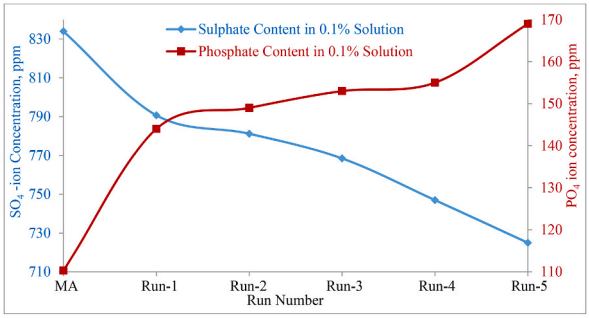

Fig. 9. Amount of recovered salt and product of GOs in the synthesis process.

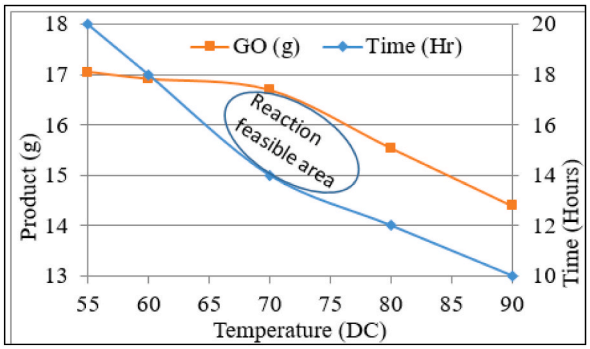

Fig. 10. Reaction times and temperature relationship and the amount of Graphene Oxide products at various times and temperature.

amount of GO has been directly related to reaction temperature and time. It could be observed that the amount of synthesized GOs.

Lower temperatures and longer reaction times yield higher amounts of GO products with smaller particle sizes, while the reverse conditions yield lesser amounts of GO products with larger particle sizes. The optimum conditions for the synthesis of GOs were found to be 65–70 °C and 14–15 h (Fig. 10). The particle size of the synthesized GOs was measured using both a particle size analyzer and SEM analysis. Particle sizes of synthesized GOs completely depended on the reaction conditions. The manipulation of reaction parameters, such as reducing the reaction temperature, increasing the reaction time, and decreasing the moisture content (leading to an increase in the pH of the reaction media), affects the size of GOs particles substantially. Specifically, lower reaction temperatures, longer reaction times, and lower moisture content tends to produce smaller GO particle sizes, as evidenced by the data presented in Table 1. Conversely, altering these conditions in the opposite direction result in larger GO particle sizes. The particle size of the generated GOs exhibits significant variation based on factors such as the extent of the temperature of oxidation reaction, duration, and pH, which greatly affect the yield of GOs, particle size, and degree of oxidation, i.e., the oxygen to carbon ratio [55].

The zeta-potential values of the GOs were determined by employing a particle size and zeta-potential analyzer. This study revealed

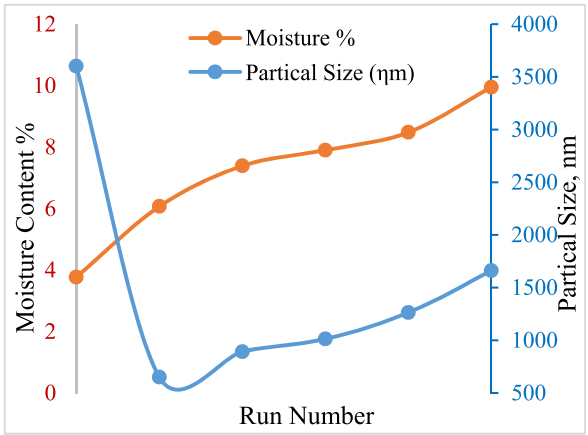

Fig. 11. Dependence of particle size of produced GOs on moisture content of the feed acids liquor.

that the measured values are dependent on the influence of reaction conditions, specifically temperature and duration of the reaction. The zeta-potential values of the produced GOs increased as lower temperatures and longer reaction periods are employed (Fig. 11). Lower values of zeta potential are obtained with higher temperature and shorter reaction period. Nevertheless, once the temperature exceeds 80 °C, the Zeta-potential value experiences a significant decline as a result of charge deactivation induced by partial reduction (Fig. 12). The zeta potential is influenced by the pH of the reaction fluid and temperature.

4. Characterization of GOs with higher oxygen to carbon ratio

4.1. FTIR-ATR spectroscopic analysis of synthesized GOs

The FTIR-ATR spectra of the purified and freeze-dried GOs samples reveal several significant absorption peaks, as depicted in Fig. 13. A broad absorption peak is observed around 3175–3230 cm^{-1}, indicating the formation of versatile hydroxyl groups (-OH) during the oxidation of graphite. This peak is absent in the spectrum of graphite in Fig. 13 (a). Additionally, there is a sharp absorption peak at around 1704–1720 cm^{-1}, which is attributed to the formation of groups carboxyl (–CO–), and another sharp peak at around 1591–1620 cm^{-1}, corresponding to the stretching and bending vibration modes of groups (-OH). Two shorter absorption peaks are observed around 1354–1394 cm^{-1} and 1237–1262 cm^{-1}, indicating the formation of etheric oxygen (C–*O*–C) bond stretching modes. Finally, there is a sharp and intense absorption peak at around 1048–1057 cm^{-1}, which corresponds to the vibrational mode of the C–O bond. These FT-IR absorption peaks provide confirmation of the formation of the oxidized form of the synthesized GO products [55–57].

4.2. UV-visible spectroscopic analysis

Fig. 14 depicts the UVvisible spectra of the raw graphite and prepared graphene oxide. The spectrum corresponding to the graphite shows no absorption peaks, as expected. All spectra of graphene oxide exhibit an absorption peak at around 242–253 nm, along with other minor peaks. The absorption peak is centered at $\lambda_{max} = 243$ for Run-1, which resembles the $\pi \rightarrow \pi^*$ transition of C═C of the graphene layer [57]. Similar peaks are observed for samples from Run-2 to Run-5 at wavelengths closer to the λ_{max} of Run-1. In addition to the broad peak, a shoulder is observed for all the graphene oxide samples. This shoulder is related to the $\pi \rightarrow \pi^*$ transition involving the C–O and >C═O groups present on the graphene sheet. Run-1 displays the presence of absorption peaks in the range of 600–800 nm [58]. These peaks are related to the presence of impurities present on the surface of the graphene oxide layer. Another interesting observation is the presence of minor peaks located in the 300–400 nm range for samples Run-3 and Run-4. The intensity of the $\pi \rightarrow \pi^*$ transition depends on two types of conjugative effects: one is related to the nanometer-scale sp^2 clusters, and the other is related to the number of chromophore units such as C–O, C═O, and C═C bonds [59]. The samples with the increased number of chromophore units show $\pi \rightarrow \pi^*$ peaks with higher intensity. The chromophore units progressively increase from sample Run-1 to Run-4. Run-5 is an exception where the intensity of the absorption maxima is reduced significantly compared to all other graphene oxide samples. Absorption spectra of the GOs also addresses the size distribution in dispersed medium. According to quantum confinement principle, the small particle sizes in microscopic scale tends to show absorption edges around lower wavelengths or higher energy and GOs with larger particle sizes show absorption edges around higher wavelength or lower energy [60,61]. GOs in case of run-1 consists of low particle sizes and sizes progressively increase in cases of run-2 to run-5. Although, the peaks at 240–250 nm are almost unshifted in runs 1–4 run-5 shows the highest λ_{max} which is indicative of its higher particle sizes. Moreover, the peak shift is very small because particles exceed the required size to effectively showcase quantum confinement effect [62].

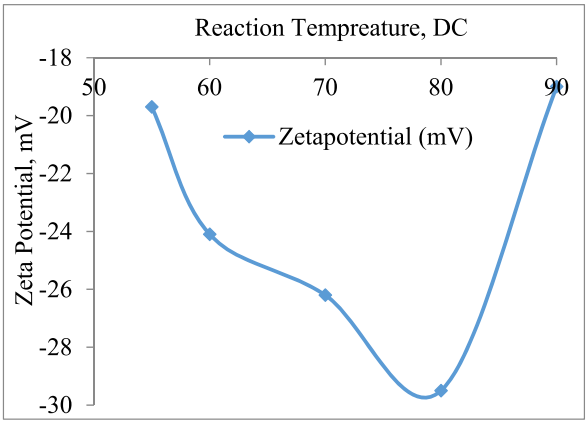

Fig. 12. Dependence of Zeta potential of synthesized GOs on temperature of the feed acids liquor.

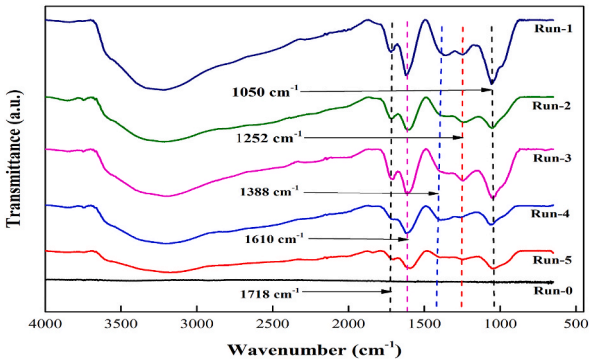

Fig. 13. FT-IR spectroscopic analysis of different graphene oxide products- (a) graphene oxide represents Run-1, (b) graphene oxide represents Run-2, (c) graphene oxide represents Run-3, (d) graphene oxide represents Run-4, (e) graphene oxide represents R-5, and (f) raw graphite represents Run-0.

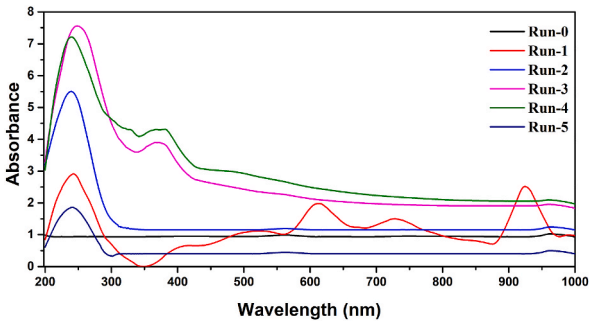

Fig. 14. UV Visible spectroscopic analysis of different graphene oxide products (a) Run-0, raw graphite, GOs of (b) Run-1 (λ_{max} value 243 nm), (c) Run-2 (λ_{max} value 240 nm), (d) Run-3 (λ_{max} value 242 nm), (e) Run-4 (λ_{max} value 240 nm) and (f) Run-5 (λ_{max} value 250 nm).

4.3. FT- Raman spectrum analysis

Fig. 15 depicts the Raman spectra of the graphite and the prepared GOs samples. Raman spectroscopy is widely used to gain insight into the structural information of carbon-based materials [63–66]. The presence of C═C bonds and conjugation leads to high Raman intensities. The spectrum of graphite shows no Raman bands, as expected. In the case of GOs, very noisy spectra are observed. However, the most prominent bands can be distinguished from these spectra at around ~1355 cm^{-1} and ~1575 cm^{-1}, corresponding to the disorder band caused by graphitic edges, also denoted as the D band, and the phase vibration of the graphite lattice, denoted as the G band, respectively [67]. The intensity of the G and D bands is highly dependent on the structure of the graphene oxide. As the disorder in the graphene lattice takes place, the D band's relative intensity increases compared to the G band. Moreover, the G band becomes broader with increased disorder in the structure of the graphene oxide. Run-1 shows a relatively higher intensity of both the G and D bands, indicating the presence of disorder in the structure of graphene oxide [68]. The G and D band were absent in the reacrion R-0 for pure graphite. Furthermore, GOs formation leaves topological defects and vacancies. Interestingly, the bands do not show any type of blue or red shift progressing from Run-2 to Run-5, which suggests the absence of amorphous graphene [69].

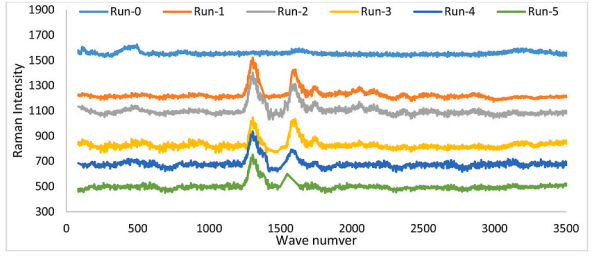

Fig. 15. FT-Raman spectroscopic analysis of different graphene oxide products- (a) Run-0, raw graphite, (b) graphene oxide of Run-1, (c) graphene oxide of Run-2, (d) graphene oxide of Run-3, (e) graphene oxide of Run-4, and (f) graphene oxide of Run-5.

4.4. SEM analysis

Fig. 16 shows the FESEM micrographs of GOs showcasing the surface morphology at different magnifications. FE-SEM micrographs indicates that different forms and sizes of GOs have been formed. GOs showed a layered structure and layer thickness were found to be at 200–260 nm, as seen from Fig. 16 (C). GOs generally have well-defined and interlinked three-dimensional graphene sheets, forming a porous network that resembles a loose sponge-like structure [70]. The wrinkled and layered flakes seen on the surface implies that the graphene layers were fully oxidized to GOs [71].

4.5. XPS analysis of synthesized GOs

XPS is a readily accessible and efficient quantitative technique employed for the determination of the oxidation state of surface of the materials. The XPS analysis conducted on the produced GO provides insights on the degree of oxidation in relation to the presence of organic functional groups incorporated into the structure of GOs [29,72]. The synthesized GOs from Run-3 and Run-5 underwent XPS analysis and are presented in Figs. 17–20.

The XPS survey scan analysis of the synthesized GOs from Run-3 has been presented in Figs. 17 and 18. In the survey scan analysis presented in Fig. 17, it was observed that the produced GOs samples contain two distinct peaks corresponding to carbon and oxygen atoms. Substantial peaks were observed in the survey scan of the XPS analysis. The observed peak, with a center at around 287.08 eV, can be attributed to the C1s peak, indicating the presence of carbon atoms. At the same time, the primary peak observed at around 533.08 eV was assigned to the O1s peak, suggesting the presence of oxygen atoms (Fig. 17. Based on the area percentage calculation, the GO contains 57.75% carbon atoms and 38.55% oxygen atoms, resulting in an oxygen-to-carbon atomic ratio of 66.7%. Carbon peak exhibited five distinct sub-peaks in the deconvoluted spectra in Fig. 18 (A), which includes both sp^3 and sp^2 carbon types, C–C/C═C bonds in GOs, observed at 284.18 eV. These bonds accounted for approximately 15.838% of the material. The peak observed at 284.99 eV in the C1s spectrum was assigned to the sp^3/σ-bond of carbon-oxygen (C–O) in C–OH bonds, representing approximately 18.718% of the overall composition. The peak observed at 286.78 eV in the C1s spectrum can be attributed to the presence of sp^3/σ-bonds between carbon and oxygen atoms in the C–*O*–C epoxide and C═O functional groups. This peak accounts for roughly 39.771% of the total spectral intensity. This observation of a C1s peak at 288.78 eV suggests the existence of sp^2/π-bonds associated with the C═O moiety in the COOH compound, accounting for approximately 17.645% of the analyzed specimen. Another C satellite peak was found at 290.98 eV, which was about 8.025% of the total composition. The analysis of the oxygen peak demonstrated the existence of three distinct sub-peaks Fig. 18 (B). The peak observed at 532.88 eV in the O1s spectrum was identified as originating from the sp^3/σ-bonds of carbon-oxygen (C–O) in various chemical groups, namely C–*O*–C epoxide, C–OH, and –C(O)OH carboxylic groups. These particular groups collectively accounted for around 61.723% of the overall composition. The peak observed at 534.68 eV in the O1s spectrum corresponds to the presence of sp^2/π-bonds in the C═O functional group, which accounts for approximately 15.096% of the total signal intensity. The presence of sp^2/π-bonds of C═O in –C(O)OH carboxylic groups, which accounted for approximately 23.18% of the sample, was confirmed by the O1s signal observed at 536.08 eV [73,74].

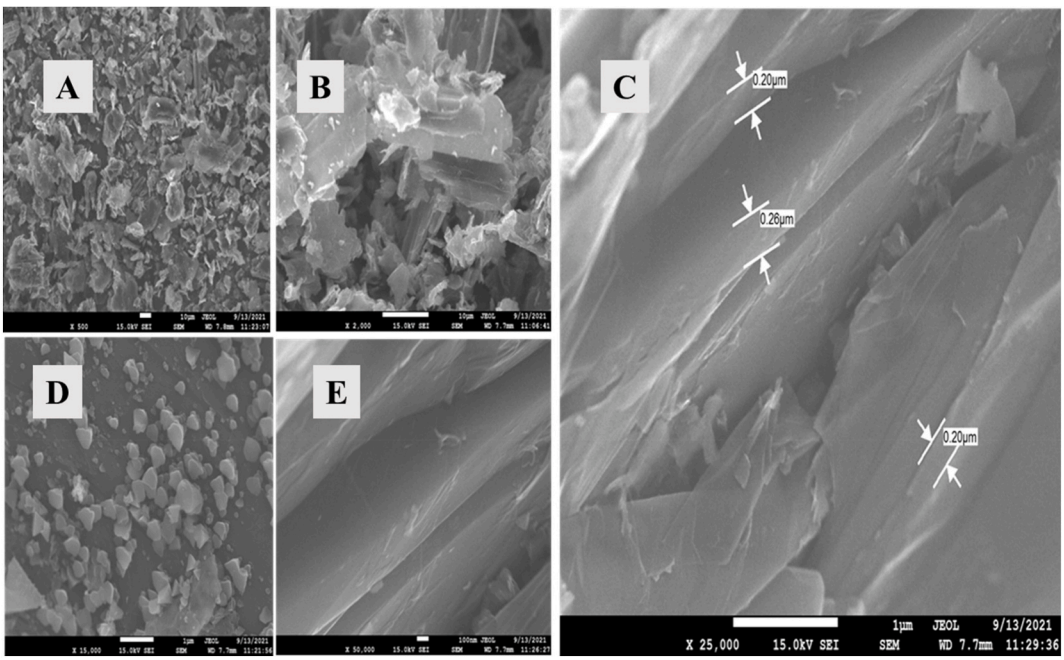

Fig. 16. Scanning electron microscopic image of R-3 GOs.

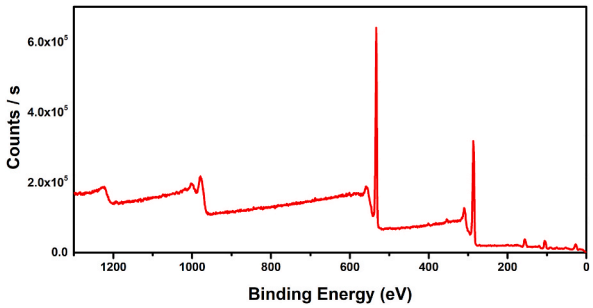

Fig. 17. XPS survey scan binding energy of Run-3 of GOs.

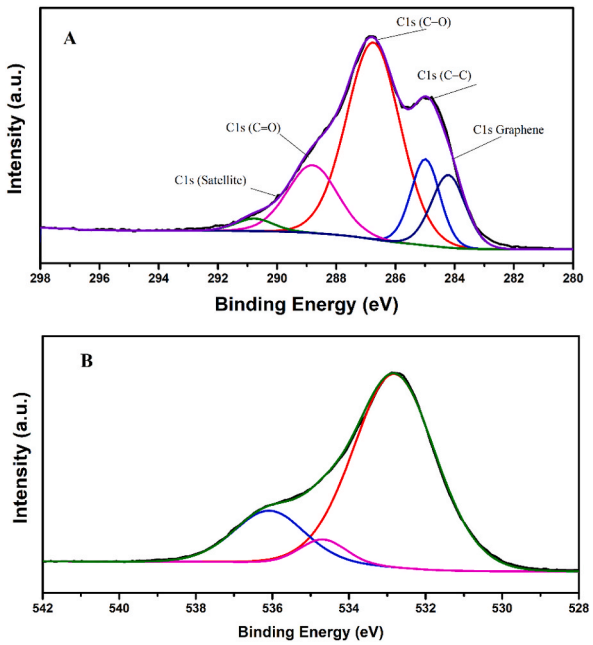

Fig. 18. XPS survey scan analysis of deconvoluted bonding energy of binding energy of (A) C-1s scan peak deconvolution of Run-3 GOs and (B) O-1s scan peak deconvolution of Run-3 GOs.

The XPS survey scan analysis of the synthesized GOs from Run-5 has been presented in Figs. 19 and 20, respectively. In the survey scan analysis presented in Fig. 19, the GOs contain two distinct peaks corresponding to carbon and oxygen atoms. The peak at approximately 287.08 eV represents the C1s peak for carbon atoms, while the peak at around 533.08 eV represents the O1s peak for oxygen atoms. Based on the area percentage calculation, the GO contains 63.88% carbon atoms and 32.69% oxygen atoms, resulting in an oxygen-to-carbon atomic ratio of 51.17%. Following the process of deconvolution, a total of five sub-peaks were obtained from the carbon peak shown in Fig. 20 (A). The peak observed at 283.88 eV in the C1s spectrum corresponds to the presence of C–C bonds in graphitic carbon. These bonds may be found in both aromatic and aliphatic carbons, indicating a mixture of sp^3 and sp^2 hybridization. The C–C bonds account for approximately 4.36% of the overall composition. The peak at 284.78 eV in the C1s spectrum corresponds to the sp^3/σ-bonds of carbon-oxygen (C–O) inside the C–OH functional groups, constituting approximately 40.40% of the total spectrum. Similarly, the peak at 286.88 eV in the C1s spectrum corresponds to the sp^3/σ-bonds of carbon-oxygen (C–O) in C–*O*–C epoxides and carbon-oxygen double bonds (C═O). This peak accounts for roughly 37.658% of the total spectral intensity. The C1s spectrum consists of peaks at 288.78 eV indicating the presence of sp^2/π-bonds of carbon-oxygen (C═O) in the carboxylic acid (-COOH) functional group representing approximately 12.019% of the overall composition. Furthermore, there exists an additional peak in the C satellite spectrum at 290.58 eV, which contributes to about 5.56% of the whole spectrum. Three sub-peaks were obtained from the deconvoluted spectra of O1s corresponding to oxygen peaks in Fig. 20 (B). O1s spectrum exhibits peak at 532.68 eV which is attributed to the sp^3/σ-bonds of carbon-oxygen (C–O) present in C–*O*–C epoxides, C–OH groups, and –C(O)OH carboxylic groups. These functional groups collectively make up around 76.05% of the overall composition [75,76]. At 534.68 eV in the O1s spectrum, the peak corresponds to the sp^2/π-bonds of the carbon-oxygen (C═O) functional group, constituting approximately 11.97% of the total spectrum. The peak at 531.08 eV in the O1s spectrum corresponds to the sp^2/π-bonds of carbon-oxygen (C═O) in carboxylic groups (-C(O)OH).

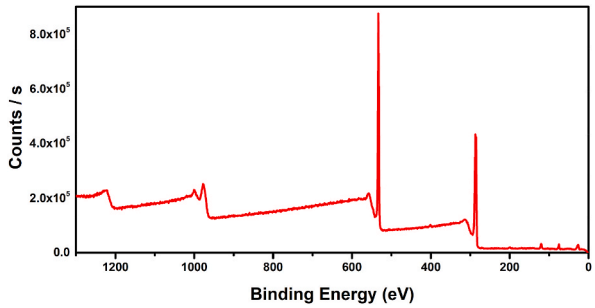

Fig. 19. XPS survey scan binding energy of Run-5 GOs.

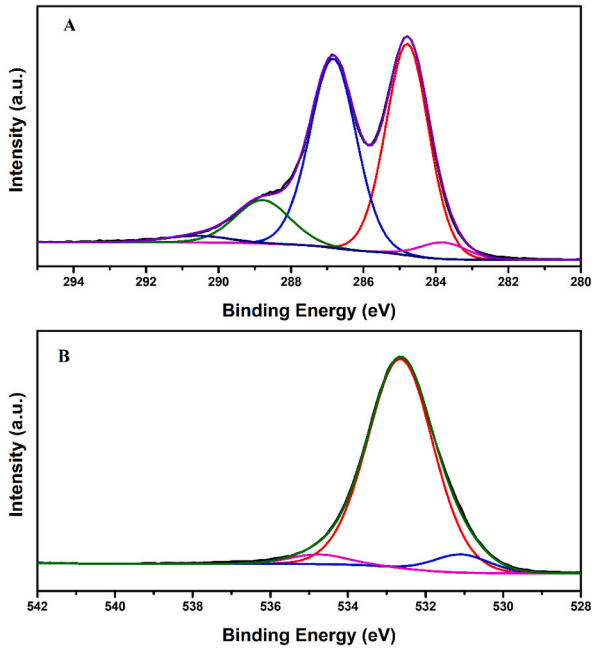

Fig. 20. XPS survey scan analysis of deconvoluted bonding energy of binding energy of Run-5 GOs. (A) C1s Scan peak deconvolution of Run-5 GOs and (B) O1s Scan peak deconvolution of Run-5 GOs.

This peak accounts for approximately 11.98% of the whole spectrum.

4.6. Thermal properties of GO

From Fig. 21, the GO is stable up to 75 °C. The loss of mass initiates beyond the temperature, and continues up to around 193 °C. At this temperature, the total mass loss is about 18%, with an observed endothermic peak in the DSC curve. This loss of mass is attributed to the water molecules trapped inside the nanolayer of GO [77]. At 193.4 °C, about 73% loss of mass of the total mass with an exothermic peak has been observed suggesting the thermal decomposition of oxygenated functional groups and the breakdown of carbon ring framework structures [76]. After that, up to 425 °C, there is no loss of mass and no change in energy is observed. Over 425 °C and up to 500 °C, a third mass loss of about 8% is observed, with an exothermic peak again. This mass loss indicates the burning of the carbon skeletons [78].

5. Correlation between the properties of synthesized GOs

Correlation analysis was performed to evaluate the relationship between the properties of the generated GOs. The results of these analyses are displayed in Table 2. Particle size of GOs exhibits a significant and positive correlation with salt recovery (0.933), dilute acid recovery (0.944), recovered acid density (0.827), moisture content (0.906), PO_4^{3-} (0.977), and potassium (0.868). Nevertheless, there is a significant negative association observed between acid recovery (−0.944) and SO_4^{2-} (−0.916). There is a significant negative association between acid recovery and salt recovery (−0.992), dilute acid recovery (−1.0), recovered acid density (−0.953), moisture

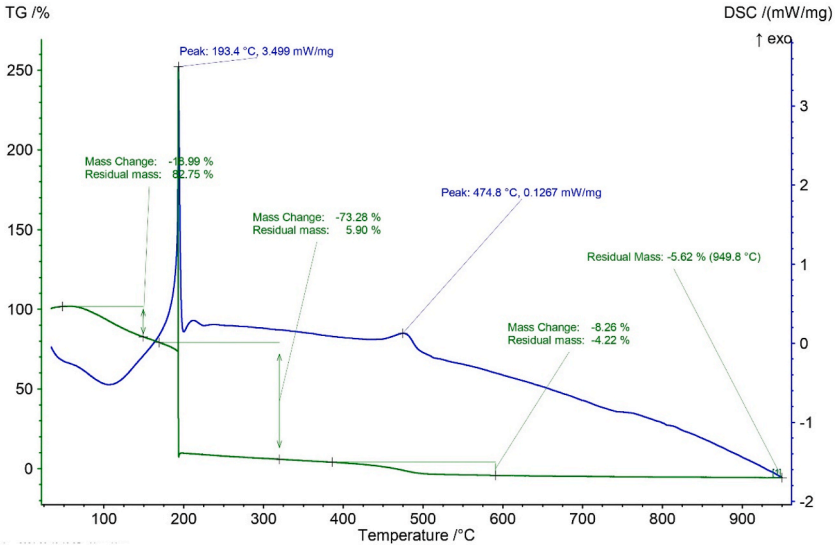

Fig. 21. Simultaneous thermal analysis (STA) of graphene oxide products of R3.

content (−0.984), PO_4^{3-} (−0.991), and potassium (−0.974). The association between acid recovery and SO_4^{2-} is quite positive, with a coefficient of 0.990. The recovery of salt exhibits a strong positive correlation with the recovery of dilute acid (0.992), the density of recovered acid (0.922), the percentage of moisture (0.994), the presence of PO_4^{3-} (0.986), and the presence of potassium (0.983). However, it shows a negative correlation with the presence of SO_4^{2-} (−0.969). The recovery of dilute acid is highly and positively connected with the density of the recovered acid (0.953), the moisture content (0.984), the PO_4^{3-} levels (0.991), and the potassium levels (0.974). However, it is adversely correlated with the SO_4^{2-} levels (−0.990). The recovered acid density exhibits a significant positive correlation with moisture content (0.935), PO_4^{3-} (0.913), and potassium (0.929), while showing a negative correlation with SO_4^{2-} (−0.982). The moisture content has a high positive correlation with PO_4^{3-} (0.973) and potassium (0.976), but a negative correlation with SO_4^{2-} (−0.970). The correlation between SO_4^{2-} and PO_4^{3-} is highly negative (−0.973), as is the correlation between SO_4^{2-} and potassium (−0.953). The correlation between PO_4^{3-} and potassium is highly positive and robust, with a coefficient of 0.946. Nevertheless, there is a weak correlation between manganese and all other features of the generated GOs.

6. Conclusions

This method has effectively produced graphene oxides (GOs) with increased oxygen-to-carbon ratios, reaching a maximum of 70.5%. The effect of reaction temperature and duration on the extent of oxidation was considered significant. The best oxidation reaction condition were achieved in respect to product yield and quality were 60–70 °C and 14–18 h. 65–70% GOs was produced at the mentioned condition. In contrast, elevated temperatures and decreased reaction time led to reduce oxidation and decreased product yield. The unreacted feed acid liquor (FAL) was successfully recycled and reused five consecutive cycles. In each recycled experiments, 80–90% of FAL was recycled and reused successfully. The properties of recycled FALs were investigated by measuring density, moisture content, pH, and ion concentration. The consecutive recycling of FALs tends to increase the moisture content about 0.5% in each recycles. Ion-chromatography (IC) was used to measure the variation in SO_4^{2-} and PO_4^{3-} ions in the FALs. The H_2SO_4 reacts with $KMnO_4$ and crystalized out from the recovered FAL faster than the phosphoric acid. So, sulfuric acid content in the makeover FALs must be greater than primary FAL However, the recovered acid slurry underwent slow dilution of 0.5% in each recycle due to water production in oxidation reaction. The alteration in concentration of the acid slurry has an impact on the size of the GO particles. The particle size of GOs were increased from 900 to 1660 nm due to the increased in moisture in the FAL. During the reaction process, SO_4^{2-} exhibits a higher degree of participation with K^+ and Mn^{2+} ions compared to PO_4^{3-} ions. The zeta potential of GOs exhibits an upward trend when the reaction temperature is increased up to 80–85 °C. The study examined how the characteristics of GOs change in response to variations in reaction parameters including temperature and time, and how these changes are related to the product yield. The impact of temperature on the reaction rate was determined to have both negative (−0.204 g/°C) and positive (+0.450 g/h) effects on the reaction time. The XPS examination revealed an oxygen-to-carbon atomic ratio of 66.7%, which correlated with the 66.9% rise in product yields observed in the experimental data. The G and D band at ~1355 cm^{-1} and ~1575 cm^{-1} in Raman spectra confirms the conversion of graphite to GOs. SEM images of GOs showed layered structure of 200–260 nm thickness. TGA showed the stability of GOs up to 75 °C. 75% of GOs was decomposed at 193 °C.

CRediT authorship contribution statement

Mohammad Amirul Hoque: Writing – review & editing, Writing – original draft, Methodology, Investigation, Formal analysis,

Table-2
Correlation among the different reaction conditions for different reaction Runs and properties of different produced GOs.

	Particle size	Zeta potential	Acid recovery	Salt recovery	Dilute acid recovery	Recovered acid density	Moisture %	SO_4^{2-}	PO_4^{3-}	Potassium	Manganese
Particle Size	1	0.372 (0.538)	0.944[a] (0.016)	0.933[a] (0.021)	0.944[a] (0.016)	0.827 (0.084)	0.906[a] (0.034)	0.916[a] (0.029)	0.977[b] (0.004)	0.868 (0.057)	0.266 (0.665)
Zeta potential	0.372 (0.538)	1	−0.046 (0.942)	0.031 (0.960)	0.046 (0.942)	−0.173 (0.781)	−0.034 (0.956)	0.011 (0.986)	0.169 (0.786)	−0.112 (0.858)	−0.559 (0.327)
Acid recovery	0.944[a] (0.016)	−0.046 (0.942)	1	−0.992[b] (0.001)	−1.000[b] (0.000)	−0.953[a] (0.012)	−0.984[b] (0.002)	0.990[b] (0.001)	−0.991[b] (0.001)	−0.974[b] (0.005)	−0.478 (0.415)
Salt recovery	0.933[a] (0.021)	0.031 (0.960)	−0.992[b] (0.001)	1	0.992[b] (0.001)	0.922[a] (0.026)<	0.994[b] (0.001)	−0.969[b] (0.007)	0.986[b] (0.002)	0.983[b] (0.003)	0.565 (0.321)
Dilute acid recovery	0.944[a] (0.016)	0.046 (0.942)	−1.000[b] (0.000)	0.992[b] (0.001)	1	0.953[a] (0.012)	0.984[b] (0.002)	−0.990[b] (0.001)	0.991[b] (0.001)	0.974[b] (0.005)	0.478 (0.415)
Recovered acid density	0.827 (0.084)	−0.173 (0.781)	−0.953[a] (0.012)	0.922[a] (0.026)	0.953[a] (0.012)	1	0.935[a] (0.020)	−0.982[b] (0.003)	0.913[a] (0.031)	0.929[a] (0.022)	0.445 (0.453)
Moisture %	0.906[a] (0.034)	−0.034 (0.956)	−0.984[b] (0.002)	0.994[b] (0.001)	0.984[b] (0.002)	0.935[a] (0.020)	1	−0.970[b] (0.006)	0.973[b] (0.005)	0.976[b] (0.004)	0.596 (0.288)
Sulphate	−0.916[a] (0.029)	0.011 (0.986)	0.990[b] (0.001)	−0.969[a] (0.007)	−0.990[b] (0.001)	−0.982[b] (0.003)	−0.970[b] (0.006)	1	−0.973[b] (0.005)	−0.953[a] (0.012)	−0.429 (0.472)
$PO4_3$–	0.977[b] (0.004)	0.169 (0.786)	−0.991[b] (0.001)	0.986[b] (0.002)	0.991[b] (0.001)	0.913[a] (0.031)	0.973[b] (0.005)	−0.973[b] (0.005)	1	0.946[a] (0.015)	0.423 (0.478)
Potassium	0.868 (0.057)	−0.112 (0.858)	−0.974[b] (0.005)	0.983[b] (0.003)	0.974[b] (0.005)	0.929[a] (0.022)	0.976[b] (0.004)	−0.953[a] (0.012)	0.946[a] (0.015	1	0.641 (0.243)
Manganese	0.266 (0.665)	−0.559 (0.327)	−0.478 (0.415)	0.565 (0.321)	0.478 (0.415)	0.445 (0.453)	0.596 (0.288)	−0.429 (0.472)	0.423 (0.478	0.641 (0.243)	1

[a] Correlation is significant at the 0.05 level (2-tailed).
[b] Correlation is significant at the 0.01 level (2-tailed).

Data curation, Conceptualization. **A.F.M. Mustafizur Rahman:** Writing – review & editing, Validation, Supervision, Methodology, Conceptualization. **Mohammad Mahbubur Rahman:** Writing – review & editing, Validation, Investigation, Formal analysis, Data curation. **Mohammad Nazrul Islam Bhuiyan:** Writing – review & editing, Methodology, Investigation, Formal analysis, Data curation. **Shirin Akter Jahan:** Writing – review & editing, Methodology, Investigation, Formal analysis, Data curation. **Md Aftab Ali Shaikh:** Writing – review & editing, Validation, Supervision, Funding acquisition, Formal analysis. **Mohammad Nurnabi:** Writing – review & editing, Validation, Supervision, Methodology, Conceptualization.

Declaration of competing interest

The authors declare that they have no known competing financial interests or personal relationships that could have appeared to influence the work reported in this paper.

Acknowledgment

The authors acknowledge the Bangladesh Council of Scientific and Industrial Research for its full support in carrying out the research work. Special thanks go to Sharmin Akter, SSO, IGCRT, BCSIR, Mahmuda Hakim, SSO, BTRI, BCSIR, and Syed Farid Uddin Farhad, PSO, PID, BCSIR, and Nasir Uddin, PSO, Dhaka laboratories, BCSIR for their instrumental support in conducting the research.

References

[1] A.K. Geim, K.S. Novoselov, The rise of graphene, Nature mater 6 (3) (2007) 183–191.
[2] K.S. Novoselov, A.K. Geim, S.V. Morozov, D.E. Jiang, Y. Zhang, S.V. Dubonos, A.A. Firsov, Electric field effect in atomically thin carbon films, Science 306 (5696) (2004) 666–669.
[3] Y. Zhu, S. Murali, W. Cai, X. Li, J.W. Suk, J.R. Potts, R.S. Ruoff, Graphene and graphene oxide: synthesis, properties, and applications, Adv. Mater. 22 (35) (2010) 3906–3924.
[4] S.C. Ray, Applications of graphene and graphene-oxide based nanomaterials, Elsevier 6 (8) (2015) 39–55.
[5] D.D. Chronopoulos, A. Bakandritsos, M. Pykal, R. Zbořil, M. Otyepka, Chemistry, properties, and applications of fluorographene, Appl. Mater. Today 9 (2017) 60–70.
[6] M. Pumera, Z. Sofer, Towards stoichiometric analogues of graphene: graphane, fluorographene, graphol, graphene acid and others, Chem. Soc. Rev. 46 (15) (2017) 4450–4463.
[7] O. Jankovský, M. Nováček, J. Luxa, D. Sedmidubský, V. Fila, M. Pumera, Z. Sofer, A new member of the graphene family: graphene acid, Chem.–Eur. J. 22 (48) (2016) 17416–17424.
[8] X. Zhang, Y. Tang, F. Zhang, C.S. Lee, A novel aluminum–graphite dual-ion battery, Adv. Energy Mater. 6 (11) (2016) 1502588.
[9] S. Mao, K. Yu, G. Lu, J. Chen, Highly sensitive protein sensor based on thermally-reduced graphene oxide field-effect transistor, Nano Res. 4 (2011) 921–930.
[10] T.Q. Trung, N.T. Tien, D. Kim, M. Jang, O.J. Yoon, N.E. Lee, A flexible reduced graphene oxide field-effect transistor for ultrasensitive strain sensing, Adv. Funct. Mater. 24 (1) (2014) 117–124.
[11] L. Liu, Y. Cheng, X. Zhang, Y. Shan, X. Zhang, W. Wang, D. Li, Graphene-based transparent conductive films with enhanced transmittance and conductivity by introducing antireflection nanostructure, Surf. Coating. Technol. 325 (2017) 611–616.
[12] J.X. Yan, Y.C. Leng, Y.N. Guo, G.Q. Wang, H. Gong, P.Z. Guo, W.P. Han, Highly conductive graphene paper with vertically aligned reduced graphene oxide sheets fabricated by improved electrospray deposition technique, ACS applied materials & interfaces 11 (11) (2019) 10810–10817.
[13] S. Pei, Q. Wei, K. Huang, H.M. Cheng, W. Ren, Green synthesis of graphene oxide by seconds timescale water electrolytic oxidation, Nat. Commun. 9 (1) (2018) 145.
[14] L. Peng, Z. Xu, Z. Liu, Y. Wei, H. Sun, Z. Li, C. Gao, An iron-based green approach to 1-h production of single-layer graphene oxide, Nat. Commun. 6 (1) (2015) 5716.
[15] W.E. Ghann, H. Kang, J. Uddin, F.A. Chowdhury, S.I. Khondaker, M. Moniruzzaman, M.M. Rahman, Synthesis and characterization of reduced graphene oxide and their application in dye-sensitized solar cells, Chem. Eng. 3 (1) (2019) 7.
[16] P. Xu, X. Liu, Y. Zhao, D. Lan, I. Shin, Study of graphdiyne biomimetic nanomaterials as fluorescent sensors of ciprofloxacin hydrochloride in water environment, Desalination Water Treat. 302 (2023) 129–137.
[17] R. Han, P. Wu, High-performance graphene oxide nanofiltration membrane with continuous nanochannels prepared by the in-situ oxidation of MXene, J. Mater. Chem. A 7 (11) (2019) 6475–6481.
[18] S. Sali, H.R. Mackey, A.A. Abdala, Effect of graphene oxide synthesis method on properties and performance of polysulfone-graphene oxide mixed matrix membranes, Nanomaterials 9 (5) (2019) 769.
[19] R. Al-Gaashani, A. Najjar, Y. Zakaria, S. Mansour, M.A. Atieh, XPS and structural studies of high quality graphene oxide and reduced graphene oxide prepared by different chemical oxidation methods, Ceram. Int. 45 (11) (2019) 14439–14448.
[20] H.L. Poh, F. Šaněk, A. Ambrosi, G. Zhao, Z. Sofer, M. Pumera, Graphenes prepared by Staudenmaier, Hofmann and Hummers methods with consequent thermal exfoliation exhibit very different electrochemical properties, Nanoscale 4 (11) (2012) 3515–3522.
[21] Y. Hua, F. Li, N. Hu, S.Y. Fu, Frictional characteristics of graphene oxide-modified continuous glass fiber reinforced epoxy composite, Compos. Sci. Technol. 223 (2022) 109446.
[22] R. Ruoff, Calling all chemists, Nat. Nanotechnol. 3 (1) (2008) 10–11.
[23] B. Paulchamy, G. Arthi, B.D. Lignesh, A simple approach to stepwise synthesis of graphene oxide nanomaterial, J. Nanomed. Nanotechnol. 6 (1) (2015) 1–4.
[24] W.S. Hummers Jr., R.E. Offeman, Preparation of graphitic oxide, J. Am. Chem. Soc. 80 (6) (1958), 1339-1339.
[25] F. Ullah-Khan, S. Mahmood, Z. Ahmad, T. Mahmood, Z.A. Nizami, Graphene oxide synthesis by facile method and its characterization, Open J. Chem. 2 (1) (2019) 11–15.
[26] D. Hou, Q. Liu, X. Wang, Y. Quan, Z. Qiao, L. Yu, S. Ding, Facile synthesis of graphene via reduction of graphene oxide by artemisinin in ethanol, Journal of Materiomics 4 (3) (2018) 256–265.
[27] H. Yu, B. Zhang, C. Bulin, R. Li, R. Xing, High-efficient synthesis of graphene oxide based on improved hummers method, Sci. Rep. 6 (36143) (2016) 1–7.
[28] N.I. Zaaba, K.L. Foo, U. Hashim, S.J. Tan, W.W. Liu, C.H. Voon, Synthesis of graphene oxide using modified hummers method: solvent influence, Procedia Eng. 184 (2017) 469–477.
[29] D.C. Marcano, D.V. Kosynkin, J.M. Berlin, A. Sinitskii, Z. Sun, A. Slesarev, J.M. Tour, Improved synthesis of graphene oxide, ACS Nano 4 (8) (2010) 4806–4814.
[30] R. Al-Gaashani, A. Najjar, Y. Zakaria, S. Mansour, M.A. Atieh, XPS and structural studies of high quality graphene oxide and reduced graphene oxide prepared by different chemical oxidation methods, Ceram. Int. 45 (11) (2019) 14439–14448.
[31] J.P.A. de Mendonça, A.H. Lima, J.C. Roldao, J.D.S. Martins, G.M. Junqueira, W.G. Quirino, F. Sato, The role of sulfate in the chemical synthesis of graphene oxide, Mater. Chem. Phys. 215 (2018) 203–210.

[32] Z. Benzait, P. Chen, L. Trabzon, Enhanced synthesis method of graphene oxide, Nanoscale Adv. 3 (1) (2021) 223–230.
[33] S. Xu, J. Liu, Y. Xue, T. Wu, Z. Zhang, Appropriate conditions for preparing few-layered graphene oxide and reduced graphene oxide, Fullerenes, Nanotub. Carbon Nanostruct. 25 (1) (2017) 40–46.
[34] M.J. Webb, P. Palmgren, P. Pal, O. Karis, H. Grennberg, A simple method to produce almost perfect graphene on highly oriented pyrolytic graphite, Carbon 49 (10) (2011) 3242–3249.
[35] S. Zhou, A. Bongiorno, Origin of the chemical and kinetic stability of graphene oxide, Sci. Rep. 3 (1) (2013) 2484.
[36] P. Noorunnisa Khanam, M.A. AlMaadeed, M. Ouederni, B. Mayoral, A. Hamilton, D. Sun, Effect of two types of graphene nanoplatelets on the physico–mechanical properties of linear low–density polyethylene composites, Adv. Manuf. Polym. Compos. Sci. 2 (2) (2016) 67–73.
[37] R.B. Capaz, Grand challenges in graphene and graphite research, Frontiers in Carbon 1 (1034557) (2022) 1–4.
[38] P. Zare, M. Aleemardani, A. Seifalian, Z. Bagher, A.M. Seifalian, Graphene oxide: opportunities and challenges in biomedicine, Nanomaterials 11 (5) (2021) 1–18.
[39] F. Liu, C. Wang, X. Sui, M.A. Riaz, M. Xu, L. Wei, Y. Chen, Synthesis of graphene materials by electrochemical exfoliation: recent progress and future potential, Carbon Energy 1 (2) (2019) 173–199.
[40] K. Parvez, Z.S. Wu, R. Li, X. Liu, R. Graf, X. Feng, K. Mullen, Exfoliation of graphite into graphene in aqueous solutions of inorganic salts, J. Am. Chem. Soc. 136 (16) (2014) 6083–6091.
[41] Z. Sofer, J. Luxa, O. Jankovský, D. Sedmidubský, T. Bystroň, M. Pumera, Synthesis of graphene oxide by oxidation of graphite with ferrate (VI) compounds: myth or reality, Angew. Chem. Int. Ed. 55 (39) (2016) 11965–11969.
[42] M. Sabbaghan, H. Charkhan, M. Ghalkhani, J. Beheshtian, Ultrasonic route synthesis, characterization and electrochemical study of graphene oxide and reduced graphene oxide, Res. Chem. Intermed. 45 (2019) 487–505.
[43] Tayyebeh Soltani, Byeong- Kyu Lee, A benign ultrasonic route to reduced graphene oxide from pristine graphite 486 (2017) 337–343.
[44] D. Ickecan, R. Zan, S. Nezir, September. Eco-friendly synthesis and characterization of reduced graphene oxide, J. Phys.: Conference Series, IOP Publishing 902 (1) (2017) 012027.
[45] M.R. Karim, H. Takehira, T. Matsui, Y. Murashima, R. Ohtani, M. Nakamura, S. Hayami, Graphene and graphene oxide as super materials, Curr. Inorg. Chem. 4 (3) (2014) 191–219.
[46] P. Parthipan, M.A. Al-Dosary, A.A. Al-Ghamdi, A. Subramania, Eco-friendly synthesis of reduced graphene oxide as sustainable photocatalyst for removal of hazardous organic dyes, J. King Saud Univ. Sci. 33 (4) (2021) 101438.
[47] B. Chandu, C.M. Kurmarayuni, S. Kurapati, H.B. Bollikolla, Green and economical synthesis of graphene–silver nanocomposite exhibiting excellent photocatalytic efficiency, Carbon Letters 30 (2020) 225–233.
[48] R. Ikram, B.M. Jan, W. Ahmad, An overview of industrial scalable production of graphene oxide and analytical approaches for synthesis and characterization, J. Mater. Res. Technol. 9 (5) (2020) 11587–11610.
[49] A.T. Habte, D.W. Ayele, Synthesis and characterization of reduced graphene oxide (rGO) started from graphene oxide (GO) using the tour method with different parameters, Adv. Mater. Sci. Eng. 2019 (2019).
[50] E. Scholz, E. Scholz, Die Karl-Fischer-Reaktion, Methoden zur Wasserbestimmung, Karl-Fischer-Titration, 1984, pp. 3–14.
[51] R.E. Smith, Ion Chromatography Applications, CRC Press, 1987.
[52] M. Sohaila, M. Saleemb, S. Ullaha, N. Saeedb, A. Afridib, M. Khanb, M. Arifb, Modified and improved Hummer's synthesis of graphene oxide for capacitors applications, Modern Electronic Materials 3 (2017) 110–116.
[53] C.V.S. Ieggli, D. Bohrer, P.C. Do Nascimento, L.M. De Carvalho, S.C. Garcia, Determination of sodium, potassium, calcium, magnesium, zinc, and iron in emulsified egg samples by flame atomic absorption spectrometry, Talanta 80 (3) (2010) 1282–1286.
[54] I. López-Garcıa, P. Vinas, C. Blanco, M. Hernandez-Cordoba, Fast determination of calcium, magnesium and zinc in honey using continuous flow flame atomic absorption spectrometry, Talanta 49 (3) (1999) 597–602.
[55] D. Prodan, M. Moldovan, G. Furtos, C. Saroși, M. Filip, I. Perhaița, D. Popa, Synthesis and characterization of some graphene oxide powders used as additives in hydraulic mortars, Appl. Sci. 11 (23) (2021) 11330.
[56] Z. Çiplak, N. Yildiz, A. Çalimli, Investigation of graphene/Ag nanocomposites synthesis parameters for two different synthesis methods, Fullerenes, Nanotub. Carbon Nanostruct. 23 (4) (2015) 361–370.
[57] P. Sahoo, L. Shubhadarshinee, B.R. Jali, P. Mohapatra, A.K. Barick, Synthesis and characterization of graphene oxide and graphene from coal, Mater. Today: Proc. 56 (2022) 2421–2427.
[58] V. Gupta, N. Sharma, U. Singh, M. Arif, A. Singh, Higher oxidation level in graphene oxide, Optik 143 (2017) 115–124.
[59] Q. Lai, S. Zhu, X. Luo, M. Zou, S. Huang, Ultraviolet-visible spectroscopy of graphene oxides, AIP Adv. 2 (3) (2012) 032146.
[60] M.R. Arefi-Rad, H. Kafashan, Pb-doped SnS nano-powders: comprehensive physical characterizations, Opt. Mater. 105 (2020) 109887, 2020.
[61] H. Kafashan, A.R. Baboukani, Electrochemically deposited nanostructured Cd-doped SnS thin films: structural and optical characterizations, Ceram. Int. 50 (3) (2024) 5717–5727.
[62] G. Chen, J. Seo, C. Yang, P.N. Prasad, Nanochemistry and nanomaterials for photovoltaics, Chem. Soc. Rev. 42 (2013) 8304–8338.
[63] S. Claramunt, A. Varea, D. Lopez-Diaz, M.M. Velázquez, A. Cornet, A. Cirera, The importance of interbands on the interpretation of the Raman spectrum of graphene oxide, J. Phys. Chem. C 119 (18) (2015) 10123–10129.
[64] D. López-Díaz, M. Lopez Holgado, J.L. García-Fierro, M.M. Velázquez, Evolution of the Raman spectrum with the chemical composition of graphene oxide, J. Phys. Chem. C 121 (37) (2017) 20489–20497.
[65] J.R. Dennison, M. Holtz, G. Swain, Raman spectroscopy of carbon materials, Spectroscopy 11 (8) (1996) 38–45.
[66] A. Coccato, J. Jehlicka, L. Moens, P. Vandenabeele, Raman spectroscopy for the investigation of carbon-based black pigments, J. Raman Spectrosc. 46 (10) (2015) 1003–1015.
[67] Fran Adar, Use of Raman spectroscopy to qualify carbon materials, Spectroscopy 37 (6) (2022) 11–15.
[68] F. Tuinstra, J.L. Koenig, Raman spectrum of graphite, J. Chem. Phys. 53 (3) (1970) 1126–1130.
[69] A.C. Ferrari, J. Robertson, Interpretation of Raman spectra of disordered and amorphous carbon, Phys. Rev. B 61 (20) (2000) 14095.
[70] B. Paulchamy, G. Arthi, B. D, A. Lignesh, Simple approach to stepwise synthesis of graphene oxide nanomaterial, J. Nanomed. Nanotechnol. 6 (1) (2015) 1.
[71] N.M.S. Hidayah, W.W. Liu, C.W. Lai, N.Z. Noriman, C.S. Khe, U. Hashim, H.C. Lee, Comparison on graphite, graphene oxide and reduced graphene oxide: synthesis and characterization, AIP conference proceedings-AIP Publishing 1892 (150002) (2017) 1–8.
[72] C. Zhang, W. Lv, X. Xie, D. Tang, C. Liu, Q.H. Yang, Towards low temperature thermal exfoliation of graphite oxide for graphene production, Carbon 62 (2013) 11–24.
[73] F.T. Johra, J.W. Lee, W.G. Jung, Facile and safe graphene preparation on solution based platform, J. Ind. Eng. Chem. 20 (5) (2014) 2883–2887.
[74] F. Priante, M. Salim, L. Ottaviano, F. Perrozzi, XPS study of graphene oxide reduction induced by (100) and (111)-oriented Si substrates, Nanotechnology 29 (7) (2018) 075704.
[75] R.M.N.M. Rathnayake, H.W.M.A.C. Wijayasinghe, H.M.T.G.A. Pitawala, M. Yoshimura, H.H. Huang, Synthesis of graphene oxide and reduced graphene oxide by needle platy natural vein graphite, Appl. Surf. Sci. 393 (2017) 309–315.
[76] D.R. Dreyer, A.D. Todd, C.W. Bielawski, Harnessing the chemistry of graphene oxide, Chem. Soc. Rev. 43 (15) (2014) 5288–5301.
[77] I. Sengupta, S. Chakraborty, M. Talukdar, S.K. Pal, S. Chakraborty, Thermal reduction of graphene oxide: how temperature influences purity, J. Mater. Res. 33 (23) (2018) 4113–4122.
[78] B. Xing, R. Yuan, C. Zhang, G. Huang, H. Guo, Z. Chen, J. Yu, Facile synthesis of graphene nanosheets from humic acid for supercapacitors, Fuel Process. Technol. 165 (2017) 112–122.